ISSN 1061-933X, Colloid Journal, 2017, Vol. 79, No. 6, pp. 715–734. © Pleiades Publishing, Ltd., 2017.
Original Russian Text © O.V. Arzhakova, A.A. Dolgova, P.A. Kechek'yan, E.G. Rukhlya, A.S. Kechek'yan, A.L. Volynskii, 2017, published in Kolloidnyi Zhurnal, 2017, Vol. 79, No. 6, pp. 679–699.

REVIEW

The Role of the Scale Factor in the Structure-Related Mechanical Behavior of Glassy Polymers

O. V. Arzhakova[a], A. A. Dolgova[a], P. A. Kechek'yan[a], E. G. Rukhlya[a], A. S. Kechek'yan[b], and A. L. Volynskii[a, *]

[a] *Department of Chemistry, Moscow State University, Moscow, 119991 Russia*
[b] *Enikolopov Institute of Synthetic Polymer Materials, Russian Academy of Sciences, Moscow, 117393 Russia*
**e-mail: volynskii@mail.ru*

Received June 27, 2017

Abstract—Literature data on the effect of the scale factor on the structure and properties of polymers have been analyzed. Two modes of the scale factor have been revealed. The first mode is related to the sizes of a polymer phase. This factor manifests itself when the polymer phase sizes become comparable with the sizes of a macromolecular coil. The second mode is directly associated with the sizes of a polymer sample and becomes detectable when investigating bulky polymer samples. The scale factor has been shown to substantially affect the structure-related mechanical behavior of loaded polymers, in particular, the stress–strain curves characterizing glassy polymers.

DOI: 10.1134/S1061933X17060035

INTRODUCTION

The study of polymer mechanical properties and their relation to structural rearrangements is an independent field of polymer science. Due to the particular applied and scientific importance of such investigations, which have been performed for many decades, their results have been described in numerous monographs, textbooks, and handbooks. It is worth noting that the performed studies have resulted in the creation of stable notions of mechanical characteristics of almost all polymers known at present. These characteristics have been presented in handbooks and are widely used in practical work by specialists dealing with different fields of science and engineering in which polymer materials are applied. However, at the end of the 20th century, the fields of industry that involve the elaboration and use of various miniature devices, including, in particular, numerous kinds of displays, began to intensely develop. The design of such devices has required the employment of nanosized polymer particles, films, and/or fibers. It has unexpectedly appeared that the known and, at first sight, well-studied properties of polymers fundamentally alter when the sizes of a polymer phase are reduced to the nanolevel. The fundamental effect of geometric parameters of macroscopic polymer objects on their mechanical responses appears to be an additional important aspect of this problem. In this review, we shall try to analyze the influence of the scale factor on the mechanical properties and structure of glassy polymers.

THE EFFECT OF POLYMER-PHASE SIZES ON THE STRUCTURE-RELATED BEHAVIOR OF GLASSY POLYMERS

Amorphous glassy polymers are widely used in different fields of science and technology, because they are, at present, produced in amounts of millions of tons. It is not surprising that, for several decades, polymer materials have been thoroughly investigated by numerous researchers, and that their fundamental properties and applied aspects have been described in detail in monographs and textbooks [1–6]. The basic mechanical characteristics of glassy polymers, such as glass-transition temperature, yield point, elongation at break, etc., have been presented in numerous handbooks. Previously, it was believed that the aforementioned characteristics were unchanged for each type of polymers.

However, at the turn of the century, a scale effect was discovered in the properties of glassy polymers [7–10]. All of the important mechanical characteristics of glassy polymers seem to depend on the sizes of a polymer phase. Let us consider the data of [11, 12] (Fig. 1) as a typical example. It is clear that the tabulated values of the most important characteristics of polystyrene (PS), which is a well-studied polymer, remain unchanged when the size of a polymer phase exceeds a value of 50–80 nm. If the polymer is "ground" to smaller sizes, its glass-transition temperature T_g and elasticity modulus begin to rapidly decrease. This decrease in T_g amounts to many tens of degrees, while the elasticity modulus may be reduced by several times

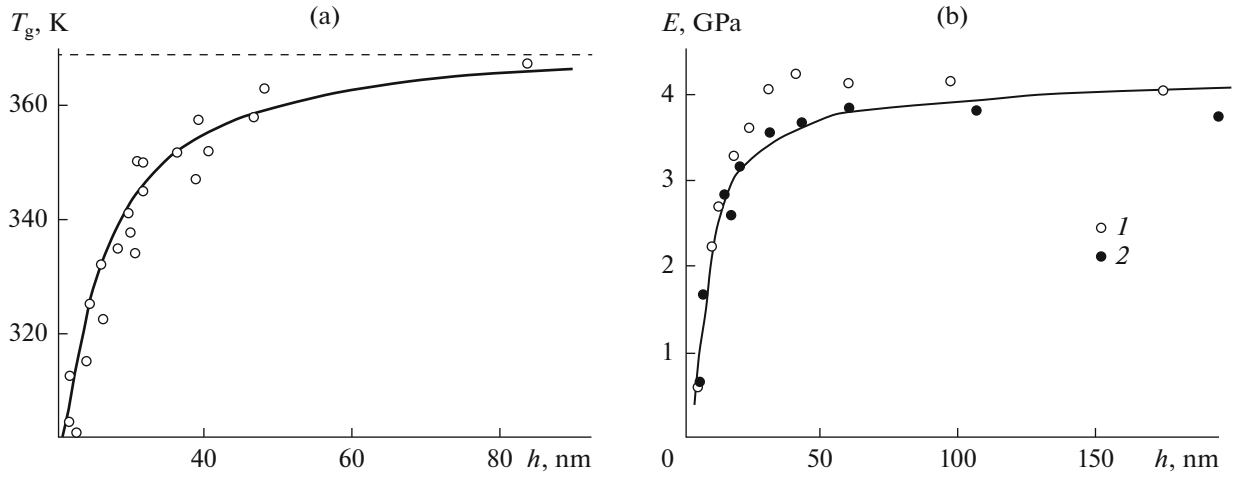

Fig. 1. Panel (a): dependence of glass-transition temperature T_g of PS films (molecular mass $M_w = (116–347) \times 10^3$) on their thickness [11]. The dashed line indicates the T_g of bulk PS. Panel (b): dependences of elasticity moduli of PS films on their thickness [12]; $M_w \times 10^{-3} = (1)$ 1800, (2) 114.

(Fig. 1). This is a general property of all glassy polymers. The mechanism of this phenomenon is not quite clear yet, and analyzing it is not a goal of this review. It should only be noted that investigations in this field are still being continued. The fact of the existence of the distinctly pronounced scale factor in itself and its strong effect on the fundamental properties of glassy polymers deserve consideration in the context of this review.

The Effect of the Scale Factor on Macroscopic Properties of Glassy Polymers

The aforementioned data on the existence of the scale factor, which affects the properties of glassy polymers, seem somewhat exotic and relevant only to nanosized objects. However, recent structural studies have suggested that highly dispersed nanosized structures are rather typical of glassy polymers; therefore, the scale factor manifests itself in many polymers and polymer-based systems [13–15].

There are known three fundamental modes of plastic deformation for solid polymers. Under different conditions, the processes of shear banding [16], crazing [17], and/or necking [18] are realized. All of them have been investigated and described in detail. As will be shown below, these processes are to a large extent governed by the aforementioned scale effect, because they comprise the stage of polymer dispersion into nanosized aggregates of macromolecules.

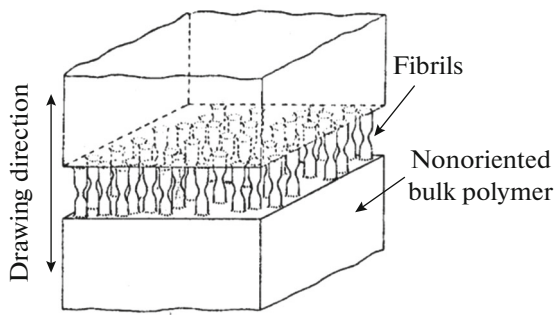

Fig. 2. Schematic representation of craze structure [28].

Self-dispersion is most clearly observed when polymers are crazed in liquid media [3, 6, 19–27]. The most important feature of polymer crazing is the fact that the development of this kind of plastic deformation is accompanied by the appearance and growth of peculiar oriented zones (crazes) in a polymer. Since crazes have a highly ordered fibrillar porous structure, they can be studied by direct microscopic methods. Such visualization of the mechanism of polymer deformation enables one to establish a direct relation between the polymer structure and properties for this kind of inelastic deformation of glassy polymers.

Within the scope of this review, it is of importance that the volume of crazes being formed appears to be filled with aggregates of oriented macromolecules (fibrils), the diameter of which amounts to a few or several tens of nanometers (Fig. 2) [28–31]. Therefore, a crazed material as a whole acquires properties (in particular, mechanical ones) atypical for amorphous glassy polymers.

Kambour and Kopp seem to have been the first to note this circumstance in their work, which was published long before the above-described scale effect was revealed in the properties of glassy polymers [32].

In [32], individual crazes were obtained by deforming glassy polycarbonate (PC) in an adsorption-active medium (AAM). A special device was used to investigate variations in the distance between the edges of an individual craze as depending on the force applied to the ends of a sample. The stress–strain curves plotted

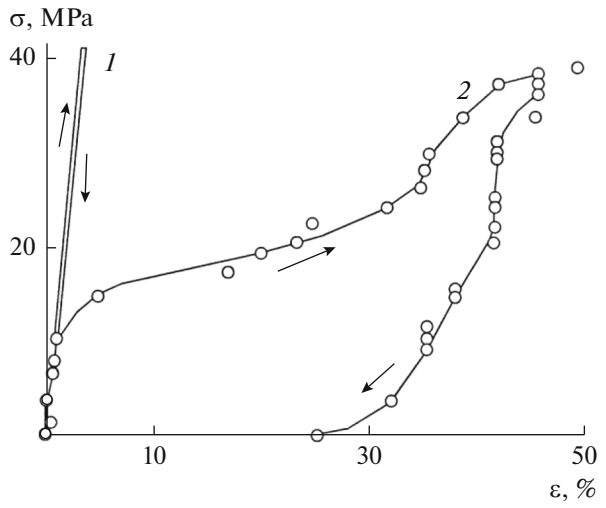

Fig. 3. Stress–strain curves for (*1*) bulk PC sample and (*2*) PC sample containing an individual craze under tensile drawing at a constant rate to a stress of 42 MPa followed by contraction [32].

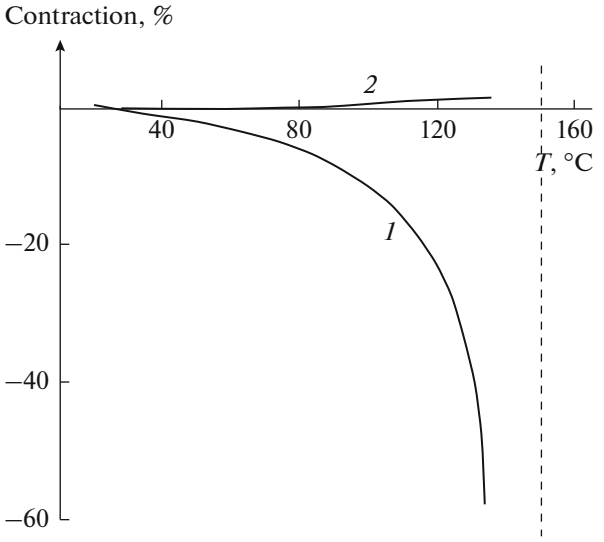

Fig. 4. Temperature dependences of relative variations in linear sizes of (*1*) crazes and (*2*) nonoriented zones between them in the direction of the drawing axis for PC samples drawn in an AAM. The vertical dashed line corresponds to the glass-transition temperature of PC [33].

in this way for an individual craze had a specific pattern, which is shown in Fig. 3. It can be seen that the yield point of the craze material is nearly three times lower than that of the initial undeformed polymer. The performance of several consecutive "deformation–restoration" cycles has shown that, as the width of an initial craze increases, the initial elasticity modulus and yield point decrease. At the same time, the energy loss in each consecutive "deformation–restoration" cycle also decreases.

At high strains, the stress–strain dependence for an individual craze is almost linear, while the deformation is completely reversible. The elasticity modulus calculated from this dependence is nearly four times lower than that for the initial undeformed sample. Thus, the mechanical properties of the "dry" material of an individual craze fundamentally differ from the properties of an initial bulk polymer.

It appears that the thermomechanical properties of crazed polymers also radically differ from the properties of bulk polymers. The peculiar unusual properties of the highly dispersed material of crazes were shown in [24] (Fig. 4). In that work, a direct microscopic method was used to measure the distances between the walls of crazes in PC as depending on the temperature of polymer sample annealing. It is well known [2] that oriented glassy polymers have their initial sizes restored in the vicinity of their glass-transition temperature. However, the material of crazes exhibits absolutely different thermomechanical behavior. As follows from Fig. 4, long before T_g is reached (actually beginning from room temperature), the craze width begins to markedly decrease, while the nonoriented zones between the crazes somewhat increase their sizes due to the thermal expansion [33]. Hence, the observed low-temperature contraction is caused by processes proceeding inside crazes or, in other words, is governed by the properties of a highly dispersed oriented polymer filling the crazes. When T_g is reached, the crazes, the width of which has already diminished by 90–95%, are "healed" and cannot be detected by direct microscopic inspections. Thus, the character of the deformation reversibility upon annealing of glassy polymers subjected to cold drawing in a liquid medium has some specific features. Amorphous glassy polymers deformed in AAMs by the crazing mechanism have their sizes almost completely restored upon annealing below the glass-transition temperature. The observed low-temperature contraction is, obviously, associated with the properties of the highly dispersed material of crazes that have formed during polymer deformation in an AAM. It can be seen that the size (scale) of a polymer phase dramatically changes the basic properties of glassy polymers.

It should be noted that anomalies in the properties of deformed polymers are observed not only in the case of crazing. Analogous anomalies are also known for polymers deformed in the absence of active media [34]. This is not surprising, because the inelastic deformation of a glassy polymer is always nonuniform over its volume. Even under the conditions of uniaxial compression or rolling, a polymer is deformed rather nonuniformly (Fig. 5) [35]. The technique of thin sections makes it possible to ascertain that PS deformed under the conditions of uniaxial compression is actually saturated with some nonuniform rectilinear formations, which cross a polymer sample and each other at different angles.

Fig. 5. Optical micrograph taken from a thin section of PS sample subjected to uniaxial compression along the vertical axis [35].

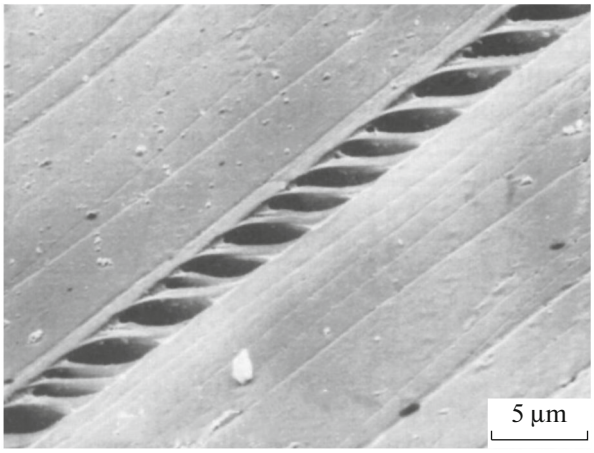

Fig. 6. Electron micrograph depicting the internal structure of a shear band [16].

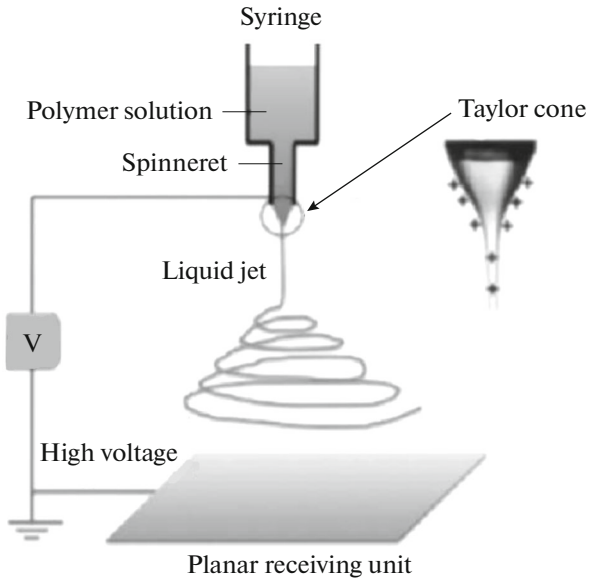

Fig. 7. Scheme of producing polymer nanofibers by electrospinning [38].

The aforementioned rectilinear structural nonuniformities have been named "shear bands." It should be noted that these shear bands fundamentally differ from the shear bands observed in low-molecular-mass solids. These bands appear to contain an oriented fibrillated polymer analogous to that observed in crazes (Fig. 6) [16, 36]. In other words, as well as a crazed polymer, a glassy polymer deformed in air by the mechanism of shear banding contains a material with nanosized structural elements. Therefore, it is not surprising that glassy polymers exhibit anomalous mechanical, thermomechanical, thermodynamic, and other properties [34, 36].

Electrospinning: A Universal Method for Nanodispersion of Polymers

The influence of the scale factor on the properties of polymers can be easily revealed by the example of nanosized fibers obtained by electrospinning (ES). At present, ES has been studied in detail, and several excellent reviews generalizing the investigations in this field are available [37–39].

Nanosized fibers are obtained by the ES method from, as a rule, semidiluted solutions [40]. A solution is extruded through a spinneret in a strong electric field (Fig. 7) to obtain a jet at the spinneret outlet. Then, the formed jet is elongated and thinned by as many as 10^5 times at a rate of nearly 10^3 s^{-1}, this leading to unfolding and orientation of polymer chains. The orientation in the jet may be recorded using birefringence [41] or Raman spectroscopy [42]. It is natural that a solvent will rapidly evaporate under these conditions. As a result, a shell and a hardened nonequilibrium matrix macrostructure are formed within a few milliseconds [43–45]. The formed shell prevents the solvent from further evaporation, and a substantial amount of it remains in a fiber. During the subsequent solvent evaporation, the fiber volume remains almost unchanged and a porous structure is often formed [46]. Thus, fibers with different degrees of heterogeneity and porosity with and without monolithic shells may be obtained by varying the conditions of ES [47–49].

The interest in nanofibers produced by ES is due to a number of their properties, such as a large specific surface area [50, 51], controllable wettability [52, 53] and rate of releasing of admixtures [54], high anisotropy of electrical conductivity [55, 56], and intense light scattering and photoluminescence [57].

Polymer nanofibers radically differ from corresponding bulky polymer samples. They exhibit size dependences of mechanical and thermodynamic properties. For example, beginning from some threshold value, the elasticity moduli of hollow fibers [58] and nanofibers produced by ES [59–63] noticeably increase, and, in addition, a shift is observed in the melting temperature [64, 65].

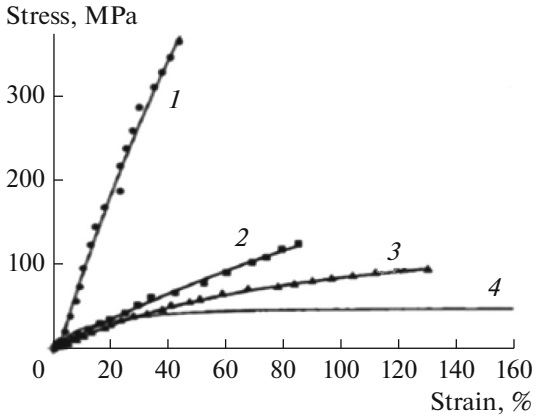

Fig. 8. Stress–strain curves for polyamide-6 fibers with diameters of (*1*) 60, (*2*) 100 and (*3*) 170 nm obtained by ES; (*4*) stress–strain curve for a bulk sample [66].

Figure 8 shows the stress–strain curves plotted for nanofibers produced by ES and for a bulk polymer drawn under the same conditions [66]. It is clearly seen that, as the fiber diameter decreases, the curves shift toward higher stresses. The strong size effect observed for nanofibers obtained by ES is common for diverse polymers.

Figure 9 presents the dependences of the relative shear modulus of PS nanofibers obtained by ES (Fig. 9a) [67] and the elasticity modulus of Nylon-6,6 nanofibers (Fig. 9b) on their diameters [60]. As follows from Fig. 9, a pronounced size effect takes place in both cases. The reasons for this effect remain unclear and cannot be explained by any single factor; however, the existence of this effect is, at present, doubtless.

Thus, it may be concluded that ES is an efficient method for producing nanosized polymer fibers. In spite of the fact that the mechanism of action of the size factor is not yet quite clear, ES may be used to show pronounced size effects in the structure-related mechanical behavior of nanosized fibers.

THE SCALE FACTOR RELATED TO POLYMER-SAMPLE GEOMETRY

Thus, nanosized polymer objects exhibit a pronounced size effect. It appears that bulky ("macroscopic") polymer samples are also characterized by a pronounced influence of sizes on their properties. This is not surprising, because the deformation of any solids and, in particular, polymers is accompanied by changes in their geometric sizes. It is obvious that a change in the geometric sizes entails a change in the surface area of a solid. The volume of a solid may remain unchanged upon deformation (as, e.g., takes place upon rubber deformation) [68]; however, its surface area always changes. In turn, a change in the area of an interfacial surface is realized via the transfer of a material from the sample bulk to the surface when the latter grows, and, on the contrary, from the surface into the bulk when it decreases. Such processes are especially intense at large deformations typical of solid polymers. Curiously enough, such mass-transfer processes have, up to the present, not attracted much attention, although understanding of these phenomena would enable one to consider many phenomena that seem well-known and studied in detail from a new point of view. Indeed, actions imposed on polymers to change their geometric sizes (primarily, large deformations) may, in essence, be considered surface phenomena because of the aforementioned mass transfer from the surface into the polymer bulk and in the opposite direction.

This aspect of polymer deformation was considered in greater detail for the first time in monograph [69].

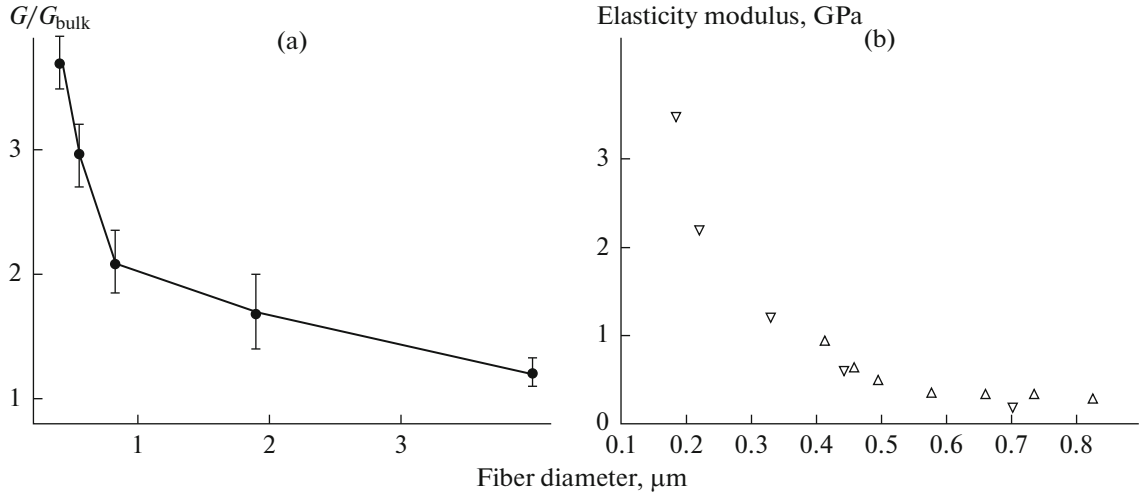

Fig. 9. Dependences of (a) relative variations in shear modulus [67] and (b) elasticity modulus [60] on fiber diameter.

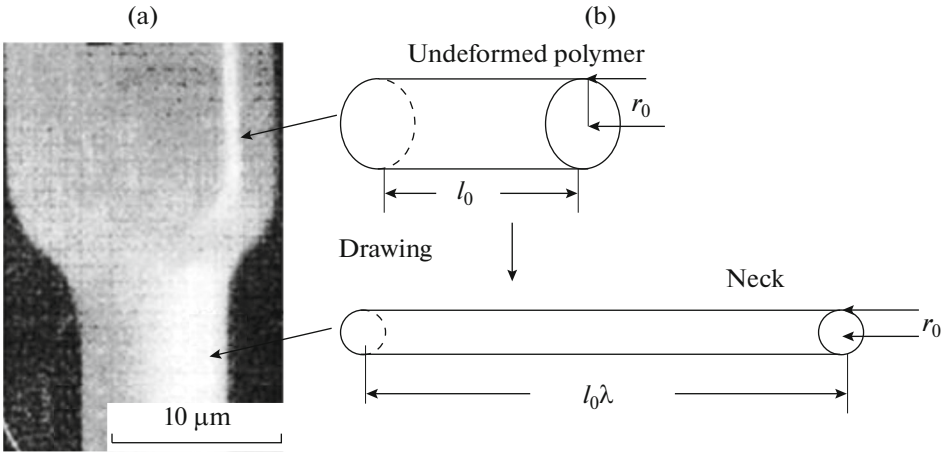

Fig. 10. Panel (a): micrograph taken from a fragment of polyester fiber in the zone of its passage into the neck and panel (b): scheme of measuring its geometric sizes during orientational drawing [78].

It is reasonable to suppose that the transport of a material from the polymer bulk to the surface and, vice versa, from the surface into the bulk must inevitably be affected by the initial geometric sizes of a polymer sample being deformed. Indeed, such transport of a material is indissolubly associated with processes proceeding in the bulk of a polymer being deformed and occurs within its volume. In this review, we shall consider the features of the processes of polymer deformation and the structural rearrangements occurring in polymers namely from the point of view of the effect of the scale factor on the aforementioned processes.

On Some Features of the Mass Transfer in the Bulk of a Polymer Being Subjected to Plastic Deformation

The development and growth or the contraction (healing) of an interfacial surface area accompany any effects on polymer systems [70]. In other words, various actions on solid polymers are associated with the transport of their material from the bulk to the surface and in the opposite direction; therefore, they may be considered to be surface phenomena.

Let us illustrate this notion by a simple example. It is well known that the deformation of an amorphous polymer below its glass-transition temperature T_g is accompanied by necking [2].

Figure 10a depicts the micrograph of a fragment of a polyester fiber in the zone of its passage into the neck [71]. It can be easily shown that the passage of a polymer into a neck is accompanied by a substantial increase in the polymer surface area. Let us consider a cylinder with initial radius r_0 and length l_0 (Fig. 10b). For simplicity, we assume that, upon the plastic elongation, the polymer volume remains unchanged. If we denote strain as λ, the constant volume condition yields the following:

$$\pi r_0^2 l_0 = \pi r^2 \lambda l_0. \quad (1)$$

From this, we obtain

$$r = \frac{r_0}{\lambda^{1/2}}. \quad (2)$$

Surface area S of a deformed fiber is equal to

$$S = 2\pi r \lambda l_0 = \lambda^{1/2} S_0, \quad (3)$$

where S_0 is the initial surface area. Or, passing to the fiber radius, we have

$$S = S_0(r_0/r), \quad (4)$$

where r_0 and r are the initial fiber radius and its current value at strain λ, respectively. Hence, it is unambiguous that, the smaller the fiber radius (other conditions being equal), the larger the fiber specific surface area (i.e., the surface area related to the volume or mass of a fiber). In the specific case illustrated in Fig. 10, surface area S_0 of a fiber fragment with length $l_0 = 1$ cm and radius $r_0 = 7.5$ μm (radius of the undeformed fiber, Fig. 10) is $S_0 = 47.1 \times 10^{-3}$ cm^2. After the fiber is drawn into a neck (for the polyester, $\lambda \approx 3$), its diameter is $r \approx 3.5$ μm (Fig. 10, the region of the neck). As follows from Eq. (4), the cold drawing of the polyester fiber has increased the initial surface area to $S = 100.8 \times 10^{-3}$ cm^2. Thus, the ordinary cold drawing of the fiber increases its surface area by more than two times. Hence, profound rearrangements relevant to the migration of the material from the bulk to the surface occur in the polymer during its deformation and from the surface into the bulk during the restoration of the sizes (contraction). However, these processes are not, at present, considered and taken into account when investigating the mechanism of polymer deformation mainly because of the absence of an efficient method for their registration.

Thus, polymer deformation via necking is accompanied by a marked change in its interfacial surface area. The development of the interfacial surface of a

glassy polymer is still more pronounced during its deformation via the crazing mechanism. The deformation (tensile drawing) of a glassy polymer in a liquid AAM may lead to polymer orientation by the crazing mechanism alone, i.e., without the involvement of the shear banding of the material [24]. The relation between the mechanical response of a polymer sample and its geometric sizes is, in the case of crazing, due to at least three causes. First, crazing is a specific kind of polymer plastic deformation, which is accompanied by the development of specific discrete structures of a plastically deformed material (crazes) in the polymer. Crazes have a nanoporous structure; therefore, they are very easy to record with the help of different microscopic methods, including optical microscopy [33]. Second, in this case, the structural features of the development of plastic deformation of a polymer may be directly juxtaposed with its mechanical response and the properties of the polymer that has passed into a highly ordered and highly dispersed state. Finally, crazing gives rise to the formation of a developed interfacial surface (with an area as large as several hundred square meters per gram) [24], which is obviously accompanied by intensed material mass transfer from the bulk to the surface, thereby making much easier the investigation of this type of material transport accompanying the deformation of a polymer sample as a whole.

Since crazing is a variant of the plastic deformation of glassy amorphous polymers, it is natural that polymer crazing in a liquid medium may be analyzed using approaches that are commonly used for the analysis of other kinds of plastic deformation [24, 72, 73]. At the same time, as has been mentioned above, in the case of crazing, the development of the inelastic deformation of polymers is, at least at early stages, realized in microvoid-containing narrow zones, i.e., crazes. This circumstance, first, makes it possible to easily record the appearance and development of crazes by microscopic methods. Second, the structural features of the development of polymer plastic deformation may, in this case, be directly juxtaposed with the mechanical response and properties of a polymer that has passed into the highly ordered and highly dispersed state.

Let us consider a typical example of this approach. Figure 11 depicts a micrograph taken with a scanning electron microscope (SEM) from an amorphous glassy poly(ethylene terephthalate) (PET) sample deformed in an AAM at room temperature. Actually, this micrograph visualizes the moment of the deformation development by the classical crazing mechanism in a liquid medium and records the state of the polymer when it reaches 100% strain. It is clearly seen that this sample indeed comprises numerous zones of a plastically deformed fibrillated material containing microvoids. At the same time, it can be seen that some of these zones (crazes) have grown through the entire cross section of the polymer sample and increase their sizes in the direction of the drawing axis (stage of widening). Some crazes, although they have grown throughout the sample cross section, have not substantially increased their sizes in the direction of the drawing axis, while others continue to grow in the direction normal to the drawing axis (stage of craze growth), which is evident from the presence of their sharp tips. It should be noted that, as the inelastic deformation of a polymer develops by the crazing mechanism, the initial bulk polymer passes into the oriented highly ordered state (craze material). Hence, the ratio between the aforementioned parts of the polymer continuously varies, thereby affecting the properties of the polymer being deformed as a whole.

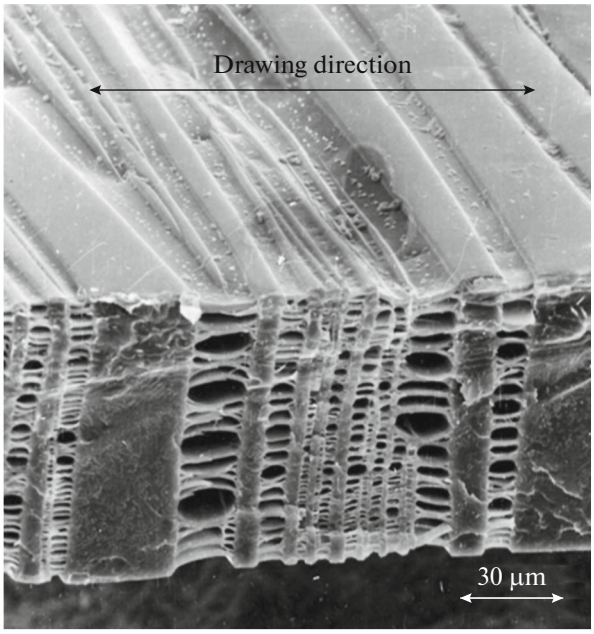

Fig. 11. SEM micrograph taken from a glassy polymer (PET) sample deformed in an AAM by 100%.

It is the nanoporous structure of the crazes developing in the course of polymer deformation in an AAM that has made it possible to reveal the direct relation between the development of individual crazes and the mechanical response of the polymer as a whole using optical microscopy (Fig. 12) [24].

Direct microscopic observations enable one to represent the development of inelastic deformation of a glassy polymer in an AAM as follows (Fig. 12). At the initial stages of polymer tensile drawing, i.e., below the yield point (region I in the stress–strain curve), some amount of crazes are nucleated on a polymer surface.

During the subsequent drawing, the nucleated crazes grow in the direction normal to the polymer drawing axis, while their very small width (fractions of micron) remains unchanged (the stage of craze growth). This process proceeds until all growing crazes have propagated through the entire cross section of a sample (region II in the stress–strain curve). This

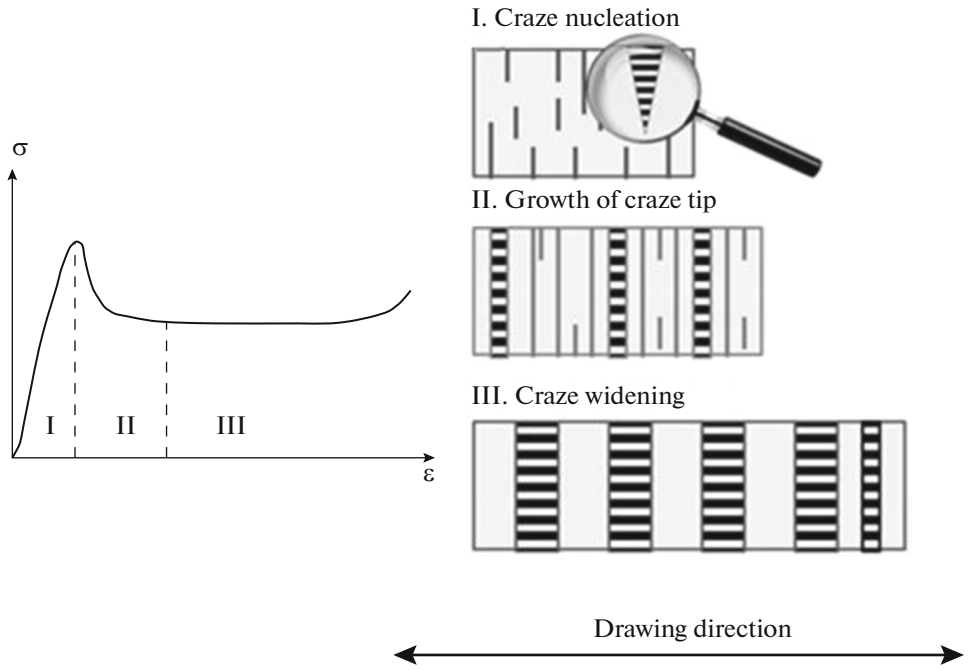

Fig. 12. Stress–strain curve for glassy polymer deformed in an AAM (on the left) and schematic representation of individual stages of polymer crazing (on the right): (I) craze nucleation, (II) craze growth, and (III) craze widening.

moment corresponds to the beginning of the plateau in the curve (Fig. 12). Then, the next stage of polymer crazing in the liquid medium—craze widening—begins. At this stage, the crazes that have grown through the entire cross section of the sample increase their sizes in the direction of the polymer drawing axis (region III in the stress–strain curve). Obviously, it is this stage at which the polymer mainly passes into the oriented fibrillated state, or, in other words, the main polymer mass transfer occurs from the bulk to the surface of fibrillar aggregates of macromolecules filling the growing crazes.

It is worth noting that the correlation of different stages of crazing with the mechanical response of a polymer being deformed was observed upon drawing not only at a constant rate, but also at a constant load (creep conditions) [74].

Thus, direct microscopic observations enable us to divide conventionally the entire process of polymer crazing in an AAM into two relatively independent stages. The first stage is the nucleation of the zones of a plastically deformed polymer (crazes) and their growth in the direction normal to the polymer drawing axis. This process proceeds until the growing crazes have propagated through the entire cross section of the polymer sample. At the second stage, after the crazes have grown throughout the cross section of the polymer, the process of their widening begins, during which the craze sizes increase in the direction of the polymer drawing axis. It is worth noting that the development of the zones of inelastic deformation and, hence, the material mass transfer into the oriented zones inside the crazes, which underlies the aforementioned development of inelastic deformation, changes its direction by 90° upon the transition from the first stage (craze growth) to the second stage (craze widening) of crazing.

Effect of the Scale Factor on the Mechanical Response of Polymer Being Deformed in Liquid Medium by the Crazing Mechanism

Thus, large inelastic deformations of polymers are accompanied by intense material mass transfer from the bulk to the surface of a sample and vice versa [69]. Let us see how these processes affect the mechanical response of a deformed polymer. Figure 13 shows the stress–strain curves for PET films deformed in an AAM (*n*-hexanol) by the crazing mechanism. In this case, the shape of the samples (double-sided spatulas) is the same, with the only difference consisting in different thicknesses of the films.

It follows from Fig. 13 that, while the yield point and the stress of the stationary development of deformation are almost independent of the sample thickness under these deformation conditions, the strain at which the stress–strain curve reaches the plateau regularly increases with the thickness (cross-sectional area) of the samples. This result corresponds to the scheme of the structural transformations accompanying polymer crazing (Fig. 12). Indeed, if the beginning of the plateau in the stress–strain curve indicates that the growing crazes have grown through the entire cross section of a polymer sample, the time required for the

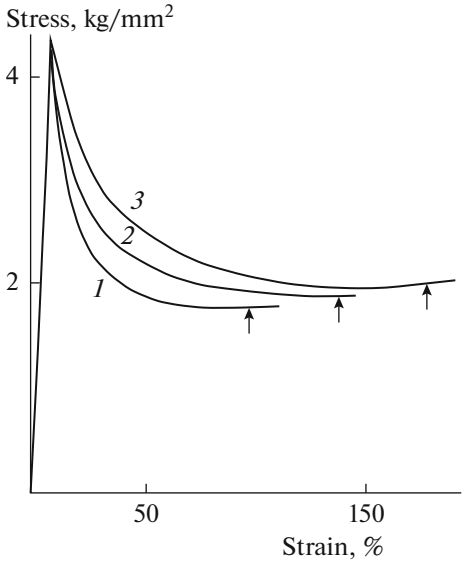

Fig. 13. Stress–strain curves for PET samples with thicknesses of (*1*) 800, (*2*) 1190, and (*3*) 1535 μm deformed in an AAM (*n*-hexanol) at a rate of 0.9 mm/min. The arrows denote the points at which the curves reach plateaus [24].

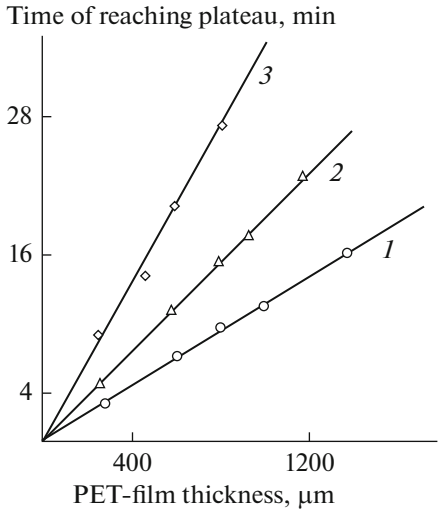

Fig. 14. Dependences of the time required for stress–strain curves to reach plateaus on sample thickness for PET drawn in (*1*) *n*-propanol, (*2*) *n*-hexanol, and (*3*) *n*-decanol. Craze growth rates calculated from these dependences are (*1*) 0.41, (*2*) 0.29, and (*3*) 0.14 mm^2/min. Strain rate is 0.9 mm/min [24].

stress–strain curve to reach the plateau characterizes the total time of their growth. It is obvious that, the larger the cross-sectional area of a sample, the longer the time required for a craze to grow through it, other conditions being equal. In this case, it becomes possible to determine the time required for crazes to grow throughout the sample cross section directly from a stress–strain curve for a polymer deformed in an AAM.

This hypothesis was verified in [24]. Figure 14 shows the dependences of the time of reaching the plateau in the stress–strain curve on the thickness of PET films being deformed in three AAMs (normal aliphatic alcohols). In all cases, these dependences are linear, thereby suggesting that craze growth rate is independent of the sample thickness. The values of the growth rate of crazes (Fig. 15) are easy to determine from the slopes of the dependences presented in Fig. 14. These values found by dividing the initial cross-sectional sizes of the samples by the time of reaching the plateau in the corresponding stress–strain curves (i.e., by the time of the craze growth throughout the sample cross section) are presented in the figure caption for Fig. 14. It follows from the data obtained that, first, a stress–strain curve provides information on the craze growth rate. In other words, the stress–strain curve for a polymer sample deformed in an AAM enables one to estimate the growth rate of plastically deformed polymer zones (crazes) through the sample cross section in the direction normal to the axis of the applied drawing stress. The data obtained unambiguously indicate an important role of the scale factor in the mechanical behavior of a polymer deformed in an AAM. Second, the craze growth rate determined from the data of Fig. 14 very strongly depends on the properties of the AAM used.

It has previously been shown that the yield point of a polymer being deformed in an AAM by the crazing mechanism depends on two main parameters—namely, the surface activity and viscosity of an AAM [24]. It is reasonable to suggest that this important

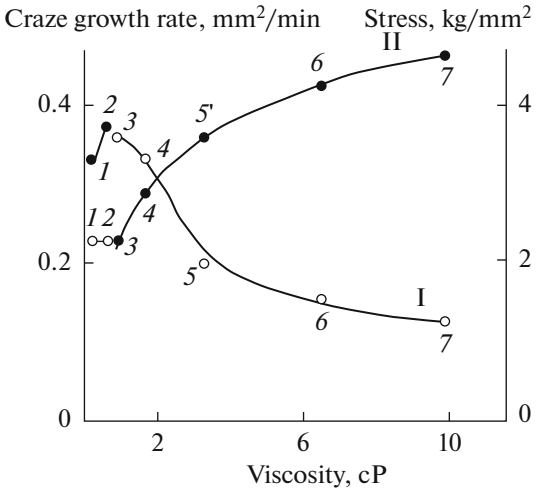

Fig. 15. Dependences of (I) craze growth rate and (II) yield point on viscosities of liquid media in which PET is drawn: (*1*) *n*-hexane, (*2*) *n*-decane, (*3*) carbon tetrachloride, (*4*) *n*-butanol, (*5*) *n*-heptanol, (*6*) *n*-decanol, and (*7*) ethylene glycol. Strain rate is 1.83 mm/min, and temperature is 32°C.

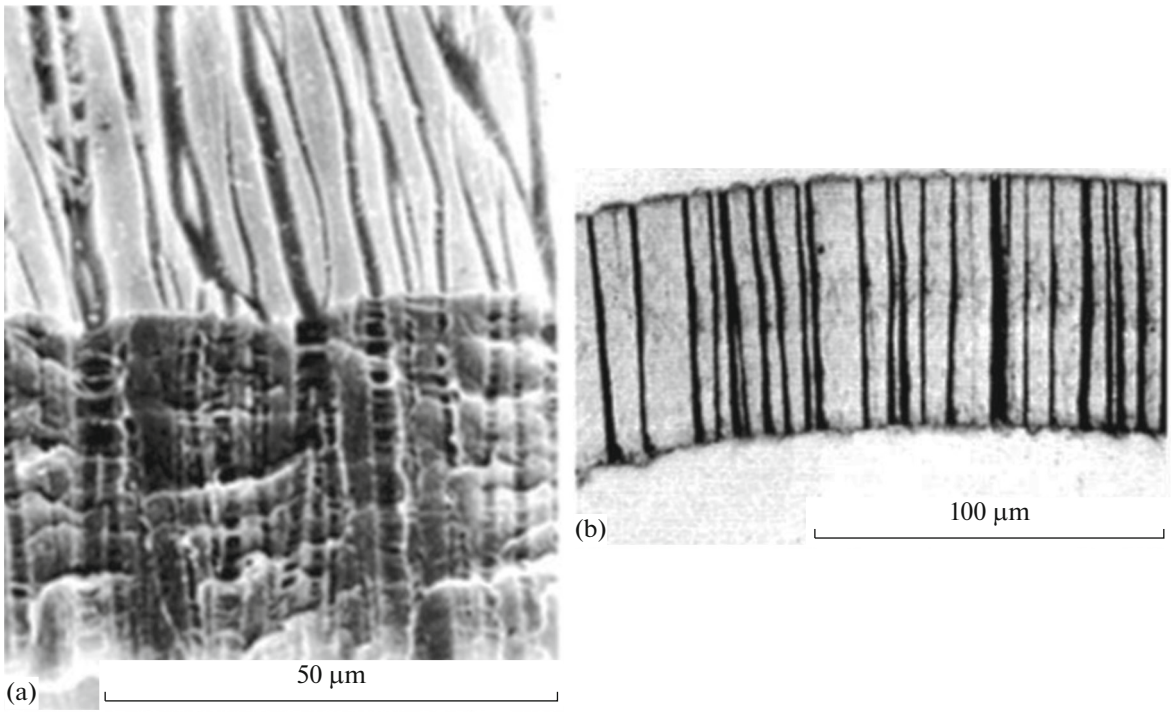

Fig. 16. Panel (a): SEM micrograph taken from PET sample 50 μm thick drawn in an AAM (*n*-hexanol) by 50% and panel (b): optical micrograph taken from a thin transverse section of a PET sample 70 μm thick drawn in *n*-hexanol by 100% [24]. Drawing performed in the horizontal direction.

characteristic of a polymer being deformed is closely related to the development of the plastically deformed polymer zones, which arise and grow in the polymer under the action of the drawing stress. This idea has been confirmed by the experimental data presented in Fig. 15.

As can be seen in Fig. 15, the craze growth rate, which, under these conditions, determines the development of the inelastic deformation in a polymer as a whole, distinctly depends on AAM viscosity: the higher the viscosity and, hence, the stronger the drag to the AAM migrating into the zone of the active plastic deformation (the tip of a growing craze), the more hindered the craze growth. In this situation, the yield point of the polymer naturally increases, because the mechanical stress is the only driving force of the crazing process as a whole. As has been shown in [24], AAS adsorbability also influences the craze growth rate, which, in turn, predetermines the yield point of a polymer being deformed in an AAM.

The Role of the Scale Factor in the Deformation of Bulky Polymer Samples by the Crazing Mechanism

It should be noted that the craze growth rates determined using the stress–strain curves for polymers deformed in AAMs have an effective character. First, at the initial stage of crazing in a liquid medium, an ensemble of crazes rather than an individual craze grows through the cross section of a sample, with the number of crazes in the ensemble depending on a number of factors [24]. Therefore, the determined values of the craze growth rate (Fig. 15) are averaged over the ensemble.

Second, the crazing of bulky polymer samples drawn in AAMs has structural features that make this process different from that schematically represented in Fig. 12. Figure 16 shows micrographs of relatively thin PET films drawn in an AAM by (a) 100 and (b) 50%.

It is clearly seen that, when relatively thin samples are drawn in an AAM, the state of affairs schematically shown in Fig. 12 is realized. At the initial stage of drawing, crazes arise in a polymer and grow throughout the cross section of a sample; then, the stage of their widening begins. A fundamentally different state of affairs is observed upon drawing of substantially larger samples (bulky samples 700 μm thick) under the same conditions (Fig. 17).

As follows from Fig. 17, when a bulky sample is deformed, crazes are nucleated on the film surface, where the polymer occurs in direct contact with an AAM, and their growth begins in the direction normal to the drawing axis. However, in contrast to thin samples, there is not enough time for crazes to grow throughout the cross section of the polymer sample by the moment at which the stress–strain curve reaches the plateau. Nevertheless, the polymer is deformed

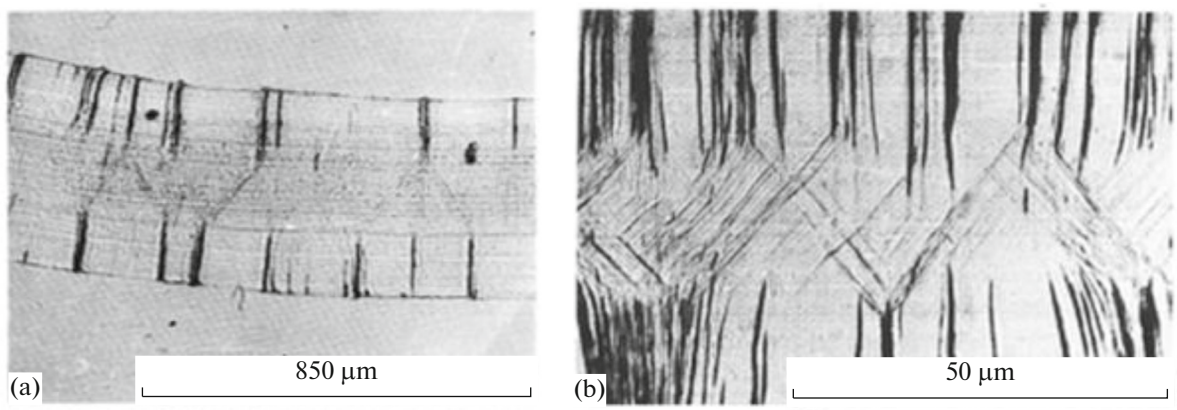

Fig. 17. Optical micrographs taken from thin sections of PET samples 700 μm thick drawn in an AAM by 15%: (a) overall view of the entire film section and (b) central part of the sample [24]. Drawing is performed in the horizontal direction.

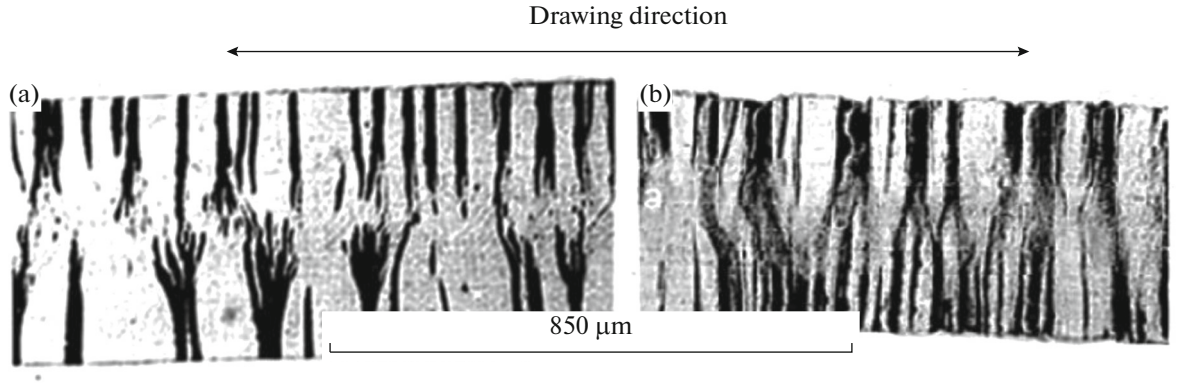

Fig. 18. Optical micrographs taken from transverse sections of PET samples 700 μm thick drawn in an AAM (*n*-hexanol) by (a) 25 and (b) 100% [24].

throughout its volume; therefore, its central region is deformed via the development of shear bands, which grow at an angle of 45°–50° with respect to the axis of polymer drawing. This is natural, because, by this moment, the AAM has not had enough time to reach the central region of the sample by moving through the set of microvoids of developing crazes.

Subsequent polymer deformation leads to a situation in which crazes grow through the sample core saturated with sear bands rather than through the uniform nonoriented polymer. This circumstance strongly affects the character of the developing deformation (Fig. 18).

It is clearly seen that crazes, which grow through the shift-band-saturated core of a deformed PET sample, begin to deviate from the direction normal to the drawing axis, curve, and branch. The SEM data (Fig. 19) indicate that, when growing crazes penetrate into the polymer region containing the shift bands, the branching process proceeds in a manner such that the tip of each individual craze splits into many (no less than ten) much thinner crazes. Deformation in an AAM gives rise to the formation of an unusual structure in bulky polymer samples: a small number of crazes are located in the surface layers, while their amount dramatically increases in the sample core.

Thus, the scale factor (in this case, the sizes of a polymer sample being deformed) has a very strong effect on the structure and, hence, the properties of a polymer deformed in an AAM.

Effect of the Scale Factor on the Competition between Shear Banding and Crazing during Polymer Deformation in an AAM

Let us consider the mechanical response of a polymer as depending on the rate of its drawing in an AAM. Figure 20 shows the stress–strain curves for an 800-μm PET film being drawn in an AAM (*n*-decanol) at room temperature and different rates. At relatively low strain rates (curve *1*), the stress–strain curves appear to have an ordinary pattern (an initial linear region followed by a yield point, a decrease in the stress, the region of a plateau, and the strain hard-

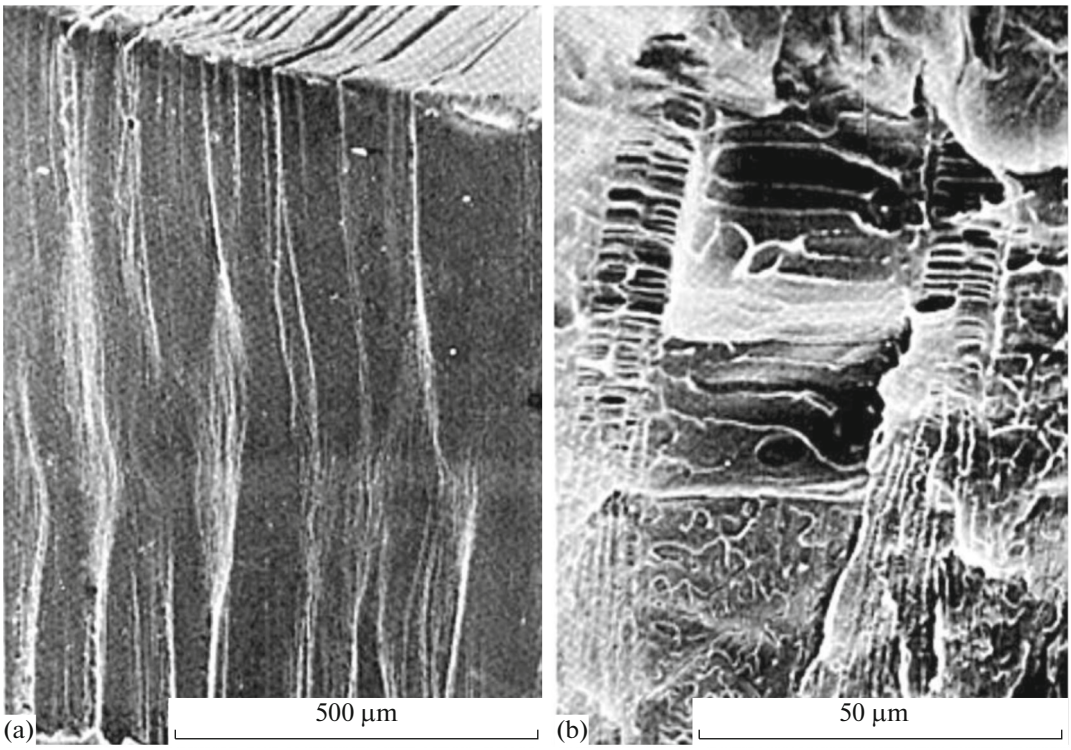

Fig. 19. SEM micrographs taken from cleavages of PET sample drawn in an AAM (*n*-hexanol) by 100%: (a) overall view of the sample section and (b) tips of crazes that have begun branching [24]. Drawing is performed in the horizontal direction.

ening). However, as the strain rate increases, the pattern of these dependences substantially changes. It can be clearly seen that the decrease in the stress in the stress–strain curves is followed by a region with a smaller slope (at high strain rates it is almost horizontal); then, one more decrease in the stress is observed followed by the strain hardening of the material.

The structural studies enable us to gain insight into the reasons for this unusual mechanical behavior of a polymer deformed in an AAM. Figure 21 presents the superposition of the results of the mechanical tests with micrographs taken from PET samples directly in the course of their drawing in an AAM.

As follows from Fig. 21, the unusual mechanical behavior (Fig. 20, curves *2*–*4*) is also accompanied by fundamental external distinctions between the samples being drawn. It is clearly seen that, at the initial stages of drawing, a neck (narrowing) arises in a sample and begins to propagate along the sample. However, the growth of the neck decelerates and almost ceases, while the subsequent inelastic deformation proceeds via the development of crazes without a noticeable lateral contraction of the material in the sample regions outside of the neck. In other words, two components of inelastic deformation of the material coexist in this case, i.e., the shear banding (necking) and crazing of the polymer in the sample fragments unoccupied by the neck at a given strain value. The contribution from each component may be easily characterized by measuring variations in the length of the growing neck (Fig. 21). It may be concluded that the main contribution to the total strain of a polymer via necking for rather bulky samples is made at the initial stages of drawing up to strains nearly corresponding to the minimum in the stress–strain curve; then, developing crazes make the main contribution to the deformation.

Thus, the rate of polymer drawing in an AAM drastically affects the character of the deformation and the mechanical response of the polymer. The mechanism of the observed phenomena will be discussed below; here, it should only be noted that geometric parameters of a deformed polymer sample exert an analogous effect on the mechanism of polymer deformation in an AAM.

Figure 22 shows a set of stress–strain curves for PET samples with different thicknesses drawn in an AAM (isopropanol) at a constant rate [33]. It is clearly seen that this set of curves is strikingly similar to the set of curves obtained for PET samples with a constant thickness but drawn at different rates (compare Figs. 20 and 22).

Moreover, all structural transformations characteristic of the curves obtained for samples with the same thickness (Fig. 20) remain retained for samples with different thicknesses.

It is worth noting that the passage from polymer deformation by the mechanism of pure crazing to deformation by the mixed mechanism of shear banding and crazing (Figs. 20–22) is also distinctly seen in the rate dependences of the yield point (Fig. 23).

As can be seen in Fig. 23, the dependence of the yield point on the strain rate is linear for PET samples deformed by the mixed mechanism (via the shear banding and crazing) as it is for polymer drawing in air (curve *1*), although it has a larger slope with respect to the abscissa axis (curves *2*–*5*). When the strain rate is decreased, the polymer passes to deformation by the mechanism of pure crazing, which is characterized by a nonlinear dependence of the yield point on the strain rate. It should be noted that the aforementioned passage depends, in particular, on the viscosity of the AAM used: the higher the viscosity, the lower the rate at which the passage occurs. This is natural, because passage from the polymer deformation by the mechanism of pure crazing to the mixed mechanism of deformation via the shear banding and crazing is, in particular, governed by the rate of craze growth through the sample cross section. The craze growth rate is, in turn, dependent on the efficiency of AAM delivery to the craze tips (the sites of active polymer deformation) by its viscous flow. It is obvious that the higher the AAM viscosity the stronger the drag to the liquid flow in narrow (nanosized) pores of a growing craze (other conditions being equal).

Thus, there are, first, several approaches to the detection of the passage from polymer deformation by the pure crazing mechanism to the mixed mechanism, namely, on the basis of analysis of stress–strain curves (Figs. 20, 22), visual inspections (Fig. 21), and the rate dependences of the yield point (Fig. 23). Second, the data presented in Figs. 19 and 21 indicate that there is some superposition of two factors, namely, the rate of polymer drawing in an AAM and the scale factor (the thickness of an initial polymer sample), variations in which cause similar changes in the mechanism of polymer deformation in an AAS.

The aforementioned superposition of the scale factor (the geometric parameters of a polymer sample) and the rate of sample drawing was considered in detail elsewhere [24]. The results of the cited investigation are presented in Fig. 24. It is clearly seen that, in the logarithmic coordinates, the deformation conditions for each used liquid medium may be divided into two regions: the region of the pure crazing (the area under curves *1*–*4*) and the region of the mixed deformation mechanism (the area over curves *1*–*4*).

The existence of the two regions with different deformation mechanisms may be explained in the following way. When a polymer sample is loaded in an AAM, crazing always begins in the sample and nucleated crazes begin to grow into the sample in the direction normal to the drawing axis. At a low loading rate and/or sample thickness, the nucleated crazes grow

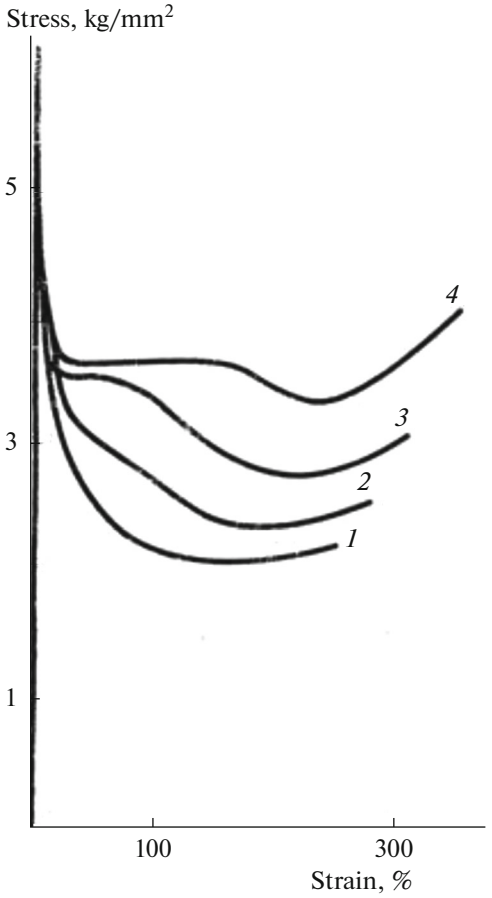

Fig. 20. Stress–strain curves for PET samples 800 μm thick drawn in an AAM (*n*-decanol) at rates of (*1*) 0.9, (*2*) 1.83, (*3*) 4.55, and (*4*) 9.46 mm/min [24].

through the entire polymer cross section; then, the stage of their widening begins in accordance with the scheme presented in Fig. 12. In other words, the process is, in this case, realized by the mechanism of pure crazing. However, if the loading rate is rather high (higher than some critical value), a stress corresponding to the polymer yield point may be reached in the core of the sample free of the growing crazes. As a result, a neck arises in the sample. The formed neck begins to propagate along the sample; however, the crazes grow in the sample zones free of the neck. As a result, the neck permanently propagates through the increasingly thinning sample core free of the crazes that would have grown through by this moment. Thus, the stress in the sample continuously decreases (see Figs. 20, 22), and the mixed deformation mechanism is realized in the polymer (the simultaneous development of the neck and the crazes). It is obvious that the sample thickness and the strain rate will have similar effects on the passage from one deformation mechanism to another. The reason for the similarity consists in the fact that, on the one hand, the sample thickness governs the time required for the crazes to grow

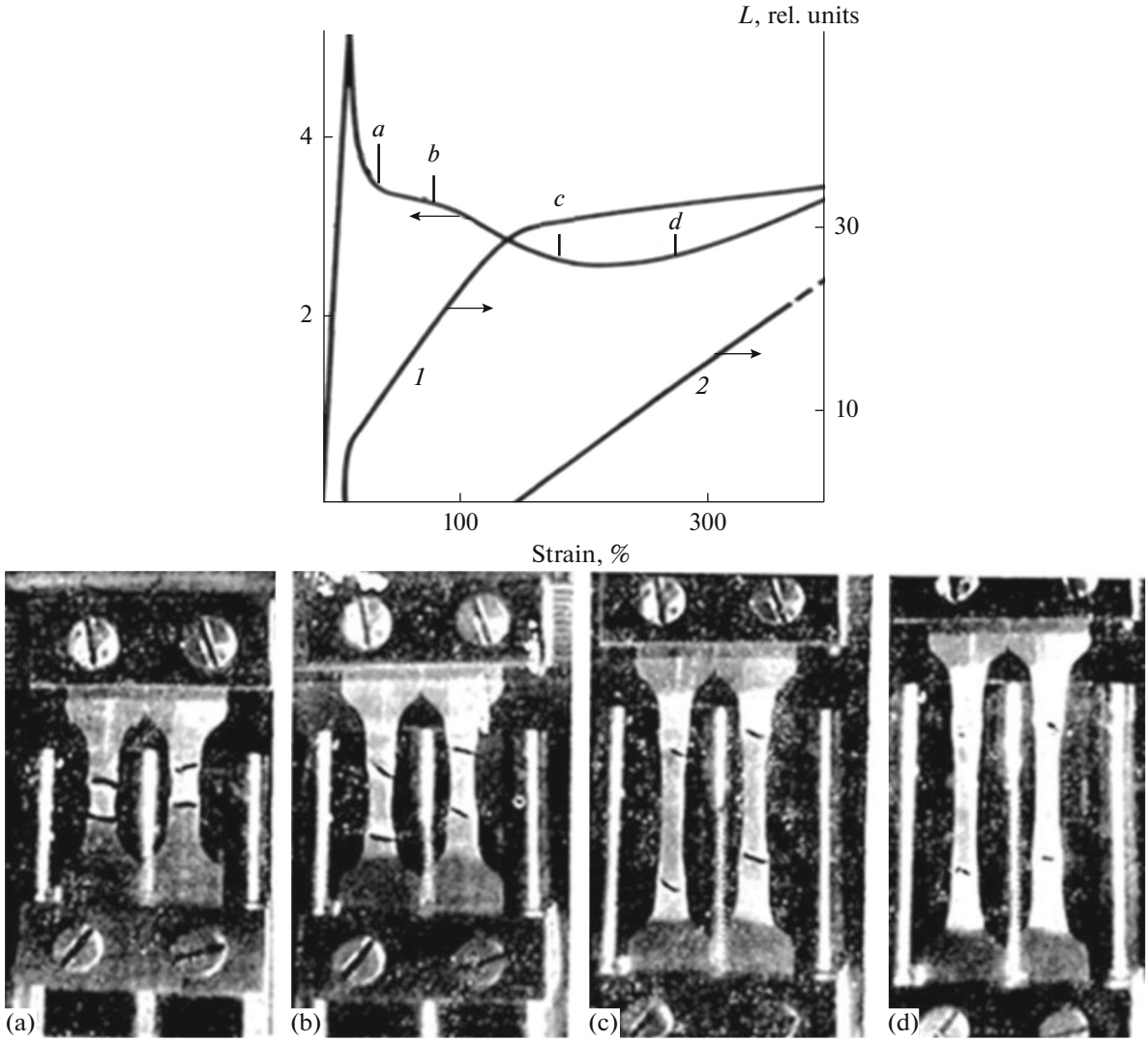

Fig. 21. Stress–strain curve for a PET sample 800 μm thick drawn in *n*-decanol at a rate of 4.5 mm/min and contributions to the strain from (*1*) neck development and (*2*) craze growth. The micrographs reflect the deformation stages denoted by literal symbols in the curve [24].

throughout the polymer cross section. On the other hand, the strain rate also affects the time of craze growth through the sample, because the craze growth rate is directly related to the mechanical stress developing in the polymer [24].

It should be noted that there is another factor that governs the above-described passage from the pure crazing of a polymer to its deformation by the mixed mechanism. Figure 24 shows that the aforementioned passage is also affected by the nature of the AAM used, because, as can be clearly seen, the curves in Fig. 24 are shifted relative to each other along the ordinate axis for different AAMs.

As has been mentioned above, the effect under consideration depends on the time of craze growth through the entire sample cross section (or, equivalently, the craze growth rate); therefore, the transport of an AAM to the sites of active polymer deformation is a necessary condition for the crazing process. It has previously been shown (Fig. 14) [24] that AAM viscosity is the main factor determining this transport, which, in turn, governs the craze growth. The influence of the viscosity can be easily taken into account using the data presented in Fig. 24. This may be illustrated as follows. Let us take the data of Fig. 24 on the deformation of PET in *n*-butanol (curve *1*) as data obtained in a "reference medium." Denote the viscosity of this AAM as η_0. Then, let us introduce a "reduction factor" in the form of η_i/η_0, where η_i is the viscosity of any of the used media (Fig. 24) and η_0 is the viscosity of the "reference liquid." The multiplication of the data on media 1–3 by the normalization factor enables us to plot a "generalized curve" (Fig. 24, curve *5*), with the data on all of the studied AAMs

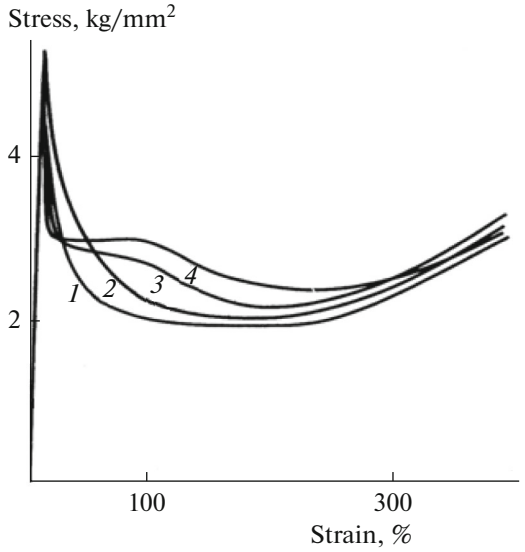

Fig. 22. Stress–strain curves for PET drawn in an AAM (isopropanol) at a rate of 18.53 mm/min. Sample thicknesses are (*1*) 300, (*2*) 575, (*3*) 900, and (*4*) 1400 μm [33].

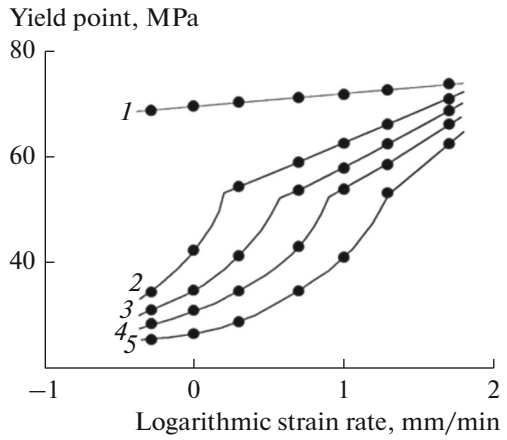

Fig. 23. Dependences of PET yield point on the rate of sample drawing in (*1*) air, (*2*) *n*-decanol, (*3*) *n*-hexanol, (*4*) *n*-propanol, and (*5*) carbon tetrachloride [24]. Film thickness is 305 μm.

accurately falling on this curve. The data obtained not only confirm the correctness of the aforementioned assumptions of the important roles of the scale factor, the rate of polymer drawing in an AAM, and the transport properties of the AAM, but also make much easier the determination of parameters that govern this or that mechanism of polymer deformation (pure crazing or the crazing/necking mixed mechanism). Hence, to determine the regions of different deformation mechanisms, it is sufficient to have experimental data on one AAM; then, the normalization procedure can be used to obtain necessary information (Fig. 24, curve *5*) without laborious mechanical tests in different AAMs.

Influence of the Scale Factor on the Stress–Strain Curve for Glassy Polymer

The mechanical response of glassy polymers under the conditions of their uniaxial drawing and compression has a rather complex character. Commonly, a stress–strain curve is represented as consisting of three main regions (Fig. 25), i.e., the so-called "elastic deformation region" (0–A), in which the deformation is geometrically reversible; the plateau region (A–B), in which a neck is formed, and the B–C region, in which the polymer that has passed into the neck is uniformly deformed [2].

This consideration of the stress–strain curve is somewhat simplified. Lazurkin was the first to mention this circumstance in his classic work [75].

Figure 26 shows the generalized stress–strain curve reported by Lazurkin as early as in 1954 [75]. In addition to the three aforementioned main regions (Fig. 25) [2], three other intervals of deformation (*a*, *b*, and *c*) are distinguished in the region of the polymer yield stress.

Figure 27 schematically represents the stages of the appearance and development of a neck during the uniaxial drawing of a glassy polymer. The aforementioned regions are juxtaposed with the profile of the stresses arising in the cross section of the polymer being

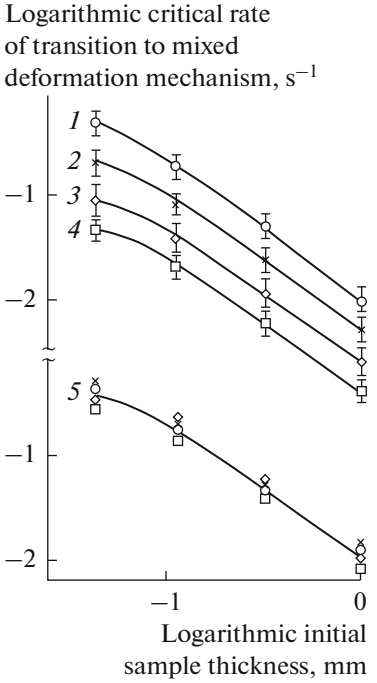

Fig. 24. Dependence of the critical strain rate, at which deformation mechanism is changed, on sample thickness for PET drawn in (*1*) *n*-butanol, (*2*) *n*-heptanol, (*3*) *n*-decanol, and (*4*) ethylene glycol; (*5*) generalized curve for the same liquid media and reduced to the viscosity of *n*-butanol [24].

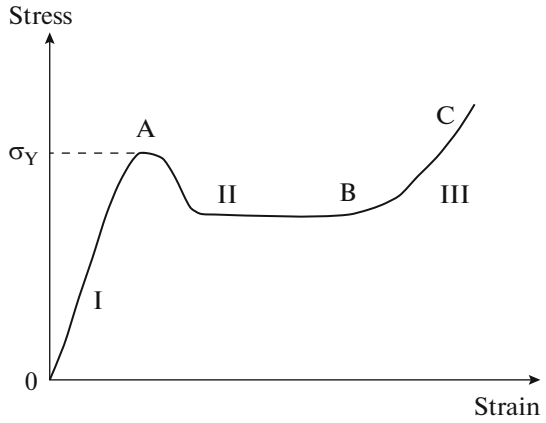

Fig. 25. Schematic representation of stress–strain curve for glassy polymer [2].

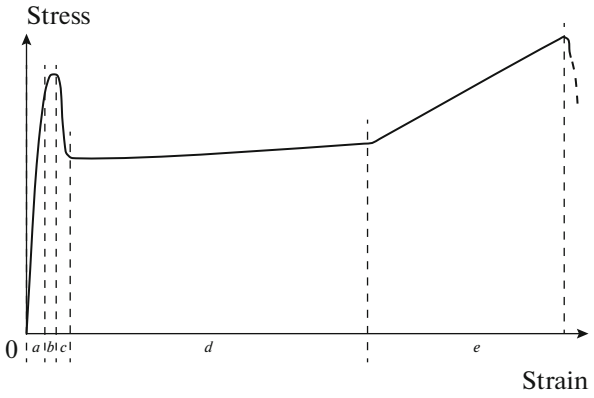

Fig. 26. Stress–strain curve for glassy polymer [75].

deformed. It follows from Fig. 27 that, at the initial stages of polymer drawing, a zone of an oriented material (interval *b* in the stress–strain curve in Fig. 26) arises. This zone growth through the cross section of the sample in the direction normal to its drawing axis (interval *c* in the stress–strain curve in Fig. 26). Only after that is the zone of an oriented polymer (neck) formed and begin to propagate along the drawing axis of the sample, until it completely passes into the oriented state (interval *d* in the stress–strain curve in Fig. 26).

The scheme depicted in Fig. 27 rather conventionally represents the morphology of the neck formation. Actually, a shear band arising in the site of the highest stress concentration in a polymer sample commonly serves as a neck nucleus (Fig. 28). It is this zone in which the nucleus of the neck is formed, which, then, propagates long the entire sample, thereby providing the effect of the strain hardening.

Thus, the initial stage of the development of the forced elastic deformation is accompanied by necking, i.e., the formation of a local zone of an oriented glassy polymer. This process is realized via the transverse (in a direction nearly normal to the drawing axis) growth of the oriented polymer zone through the entire cross section of the polymer sample. It is worth noting that, whereas all three stages of the development of the forced elastic deformation (the elasticity region, in which the deformation is geometrically reversible; the plateau region, in which the neck develops; and the region, in which the zone of the polymer that has passed into the neck is uniformly deformed [2]) have been investigated in detail, the process of the aforementioned transversal growth of the neck nucleus remains to be studied. This section is devoted to the description and analysis of the literature data on the peculiarities of the initial stages of the development of the forced elastic deformation, at which the zones of the oriented polymer are formed and propagate in the direction normal to the drawing axis.

The experimental investigation of the growth of oriented material zones upon tensile drawing of a glassy polymer is a serious problem. The matter is that these zones are nucleated in the sites of stress concentration. Such concentrators are randomly distributed in the polymer bulk; therefore, the localization of these zones cannot be predicted in advance. Moreover, such zones arise and propagate very rapidly, especially at a high rate of polymer tensile drawing. Therefore, the kinetics of the forced rubberlike deformation is commonly characterized by analyzing the temperature and rate dependences of the yield point of a polymer. In other words, the characteristics obtained in this way (activation energy or activation volume) are averaged and related to the "overall" value of the yield point with no possibility of analyzing separate stages denoted as intervals *a*, *b*, and *c* in Figs. 26 and 27.

Thus, the forced elastic deformation of a polymer at the necking stage has some peculiarities, which affect the pattern of the stress–strain curve. The onset of the polymer strain softening (the deviation of the first region of the stress–strain curve from the linearity) and the maximum and decrease in the stress correspond to the necking process, during which the zone of an oriented polymer nucleus growth through the cross section of a sample being deformed.

The inelastic deformation of a polymer via necking under tensile drawing in air is not the only method available for the development of a stable molecular orientation in it. In this connection, it should be noted that the shear banding with necking and the crazing of a polymer in liquid media have much in common. Indeed, Fig. 29 presents a series of stress–strain curves for PET deformed in several liquid media by the crazing mechanism and in air via necking. It is clearly seen that, during deformation both in air (Fig. 29, curve *1*) and in different liquid media (curves *2–9*), the stress–strain curves are similar: there are a pronounced linear region of elastic deformation, a yield point, a decrease in the stress, and a plateau.

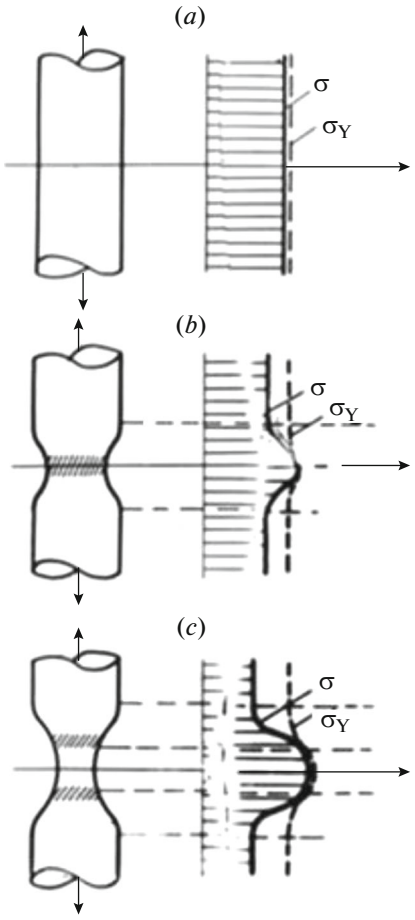

Fig. 27. Schematic representation of neck formation during cold polymer tensile drawing at a constant rate: (*a*) moment of necking onset, (*b*) stage of neck formation, and (*c*) stage of neck development [75]. Literal symbols correspond to the points in the stress–strain curve presented in Fig. 26.

It is worth noting that the data presented in Fig. 29 were obtained using standard film samples prepared as double-sided spatulas 100 μm in size with gage sizes of 6 × 20 mm. It has been shown above (Fig. 12) [24] that, when a sample is crazed in liquid media, the decrease in the stress is associated with the craze growth through its cross section in the direction normal to the drawing axis. The growth of the zone of a plastically oriented material (craze) through the sample cross section obviously depends on the sizes of the cross section, with this dependence being reflected in the pattern of the stress–strain curve. Moreover, the stress–strain curve provides information on the craze growth rate, which, in turn, is related to the properties of a liquid medium (Figs. 14, 15). It is reasonable to suppose that variations in the sample geometry must affect the mechanical response of a polymer.

This assumption is confirmed by experimental data on the deformation of 15-μm PET fibers in liquid media by the crazing mechanism and in air via necking

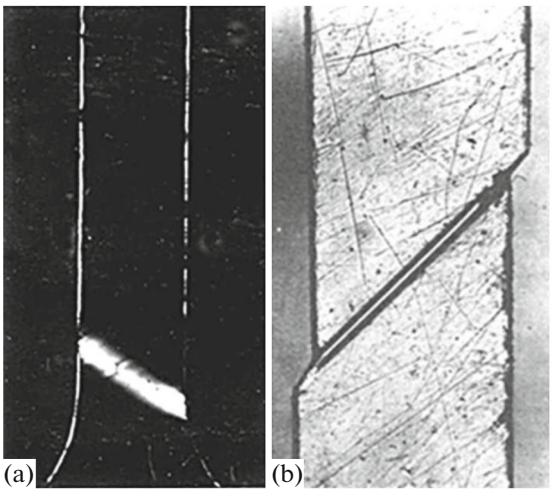

Fig. 28. Panel (a): shear bands arising at initial stages of poly(vinyl alcohol) film drawing (optical micrograph taken using crossed polaroids) [75] and panel (b): SEM micrograph of PS film [16].

[76]. The corresponding stress–strain curves are presented in Fig. 30.

It is clearly seen that all features of the stress–strain curves remain preserved for individual fibers of the glassy polymer deformed both in air and in liquid media: the elasticity region, yield point, plateau region, and strain hardening are observed. However, a decrease in the stress after reaching the yield point is actually absent irrespective of the mechanism of polymer deformation. As follows from Fig. 30, the decrease in the stress observed in the stress–strain curves is almost absent for fibers deformed both in a liquid medium (by the crazing mechanism) and in air (with the formation and development of a neck). Obviously, this is related to the small cross-sectional area of the initial polymer sample. At such a small cross-sectional area of the sample, the zone of the plastically deformed polymer (shift band or craze) grows so rapidly that the decrease in the stress "has no time" to manifest itself in the stress–strain curve.

The scale effect is still more pronounced in the mechanical tests of fibers produced by the ES. This is not surprising, because the fiber diameter is, in this case, equal to several tens or hundreds of nanometers.

Figure 31 shows the stress–strain curve for a PS fiber obtained by ES [77]. The first to be noted is the unusual mechanical behavior of PS fibers at room temperature. It is well known that PS is a brittle polymer incapable of substantial deformations at room temperature (under these conditions, its elongation at break is 1–2%). The mechanical behavior of PS dramatically changes upon passing to nanoscopic sizes. The polymer acquires plasticity and capability for marked inelastic deformations. PS is deformed with the formation of a pronounced neck, while its stress–

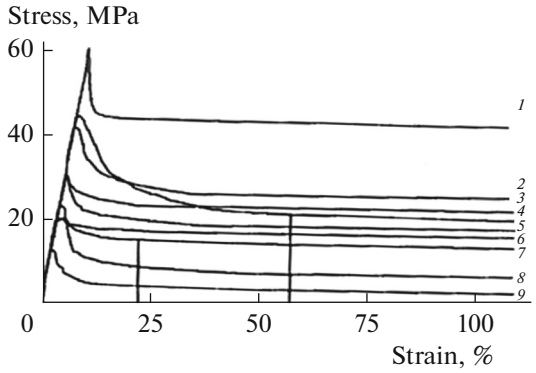

Fig. 29. Stress–strain curves for PET drawn at room temperature in (*1*) air, (*2*) ethylene glycol, (*3*) *n*-heptane, (*4*) oleic acid, (*5*) formamide, (*6*) triethylamine, (*7*) *n*-propanol, (*8*) $CC1_4$, and (*9*) butyl iodide [69].

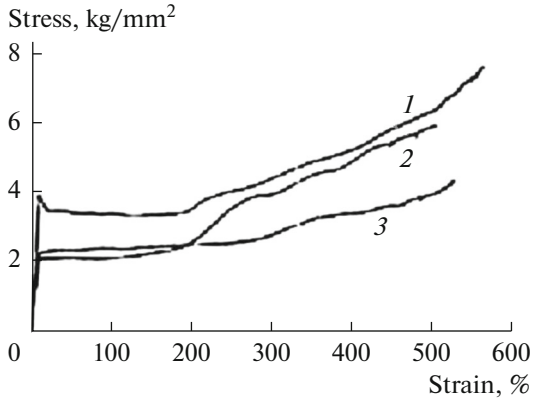

Fig. 30. Stress–strain curves for individual PET fibers 15 μm in diameter drawn in (*1*) air, (*2*) 1 : 7 butanol–water mixture, and (*3*) isopropanol [76].

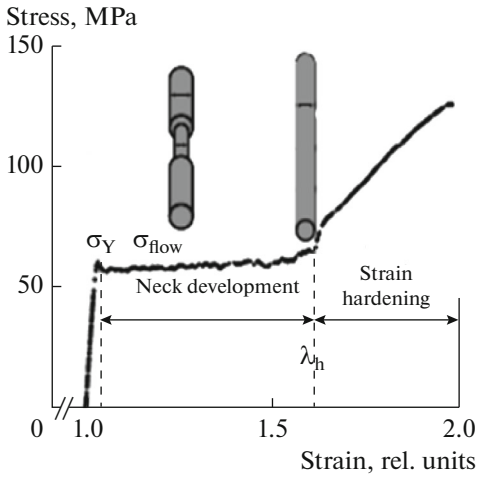

Fig. 31. Stress–strain curve for a PS fiber 200 nm in diameter obtained by ES [77].

strain curve exhibits all three regions characteristic of the glassy state (Fig. 31). At the same time, it is clearly seen that the region of a decrease in the stress after reaching the yield point is absent in the stress–strain curve of PS fibers. The study of a large set of PS fibers with diameters of 150–6000 nm has shown both the plastic behavior of the polymer and the absence of a decrease in the stress after reaching the yield point [77].

Thus, the scale factor strongly affects the structure-related mechanical behavior of glassy polymers and must be taken into account when they are used in practice.

CONCLUSIONS

The analysis of the published data evidences that the scale factor (variations in sizes) has a very strong effect on the structure and properties of polymers. This effect has, at least, a dual character. First, a decrease in the sizes of a polymer phase to those comparable with the sizes of an undisturbed macromolecular coil leads to fundamental changes in the basic characteristics of a polymer, such as its glass-transition temperature and elasticity modulus. A bulk polymer that contains zones comprising nanosized elements (e.g., crazes) drastically changes its macroscopic properties and exhibits a structure-related mechanical behavior atypical for the glassy state (a low elasticity modulus, large reversible deformations, low-temperature (below glass-transition temperature T_g) restoration of sizes, etc.). Second, there is a scale effect related to the geometry of a polymer sample being deformed. In this case, the mechanism of deformation and structure of a final material may be different depending on the sizes (scale) of a polymer sample. Stress–strain curves have been found to fundamentally depend on the sizes of a polymer sample. The aforementioned effects must be taken into account when solving practical problems relevant to the application of polymers.

ACKNOWLEDGMENTS

This work was supported by the Russian Science Foundation, project no. 17-13-01017.

REFERENCES

1. Bartenev, G.M. and Frenkel', S.Ya., *Fizika polimerov* (Polymer Physics), Leningrad: Khimiya, 1990.
2. Kuleznev, V.N. and Shershnev, V.A., *Khimiya i fizika polimerov* (Polymer Chemistry and Physics), Moscow: KolosS, 2007.
3. Ward, I.M. and Sweeney, J., *An Introduction to the Mechanical Properties of Solid Polymers,* Chichester: Wiley, 2004.
4. Perez, J., *Physics and Mechanics of Amorphous Polymers*, Rotterdam: A.A. Balkema, 1998.

5. Bartenev, G.M. and Zelenev, Yu.V., in *Entsiklopediya polimerov* (Encyclopedia of Polymers), Moscow: Sovetskaya Entsiklopediya, 1972, vol. 1.
6. Argon, A.S., *The Physics of Deformation and Fracture of Polymers*, Cambridge: Cambridge Univ. Press, 2013.
7. Keddie, J.L., Jones, R.A.L., and Cory, R.A., *Europhys. Lett.*, 1994, vol. 27, p. 59.
8. Terekhin, V.V., Zaitseva, A.V., Dement'eva, O.V., and Rudoy, V.M., *Colloid J.*, 2013, vol. 75, p. 720.
9. Rudoy, V.M., Dement'eva, O.V., Yaminskii, I.V., Sukhov, V.M., Kartseva, M.E., and Ogarev, V.A., *Colloid J.*, 2002, vol. 64, p. 746.
10. Dement'eva, O.V., Zaitseva, A.V., Kartseva, M.E., Ogarev, V.A., and Rudoy, V.M., *Colloid J.*, 2007, vol. 69, p. 278.
11. Forrest, J.A. and Dalnoki-Veress, K., *Adv. Colloid Interface Sci.*, 2001, vol. 94, p. 167.
12. Huang, R., Stafford, C., and Vogt, B., *J. Aerospace Eng.*, 2007, vol. 20, p. 38.
13. Wang, H., Chang, T., Li, X., Zhang, W., Hu, Z., and Jonas, A.M., *Nanoscale*, 2016, vol. 8, no. 32, p. 14950.
14. Mundra, M.K., Donthu, S.K., Dravid, V.P., and Torkelson, J.M., *Nano Lett.*, 2007, vol. 7, p. 713.
15. Venkatesan, S. and Basu, S., *J. Mech. Phys. Solids*, 2015, vol. 77, p. 123.
16. Li, J.C.M., *Polym. Eng. Sci.*, 1984, vol. 24, p. 750.
17. Donald, A.M., in *The Physics of Glassy Polymers*, Haward, R.N. and Young, R.J., Eds., Dordrecht: Springer Netherlands, 1997.
18. Narisawa, I., *Prochnost' polimernykh materialov* (Strength of Polymer Materials), Tovmasyan, Yu.M., Ed., Moscow: Khimiya, 1987.
19. Kramer, E.J., *J. Macromol. Sci.*, Part B, 1974, vol. 10, p. 191.
20. Kramer, E.J., *Adv. Polym. Sci.*, 1983, vols. 52–53, p. 1.
21. Friedrich, K., *Adv. Polym. Sci.*, 1983, vols. 52–53, p. 225.
22. Kramer, E.J. and Berger, L.L., *Adv. Polym. Sci.*, 1990, vols. 91–92, p. 1.
23. Kambour, R.P., *J. Polym. Sci., Macromol. Rev.*, 1973, vol. 7, p. 1.
24. Volynskii, A.L. and Bakeev, N.F., *Solvent Crazing of Polymers,* New York: Elsevier, 1995.
25. Narisawa, I. and Jee, A.F., in *Material Science and Technology. Vol. 12. Structure and Properties of Polymers*, Thomas, E.L., Ed., Weinheim: Wiley-VCH, 1993, p. 701.
26. Grellmann, W. and Seidler, S., *Deformation and Fracture Behavior of Polymers*, Berlin: Springer, 2001.
27. Yoshida, S., *Deformation and Fracture of Solid-State Materials: Field Theoretical Approach and Engineering Applications*, New York: Springer, 2015.
28. Passaglia, E., *J. Phys. Chem. Solids*, 1987, vol. 48, p. 1075.
29. Basu, S., Mahajan, D.K., and Van der Giessen, E., *Polymer*, 2005, vol. 46, p. 7504.
30. Starke, J.U., Schulze, G., and Michler, G.H., *Acta Polym.*, 1997, vol. 48, p. 92.
31. Michler, G.H., in *Deformation and Fracture Behaviour of Polymers*, Grellmann, W. and Seidler, S., Eds., Berlin: Springer, 2001, p. 193.
32. Kambour, R.P. and Kopp, R.W., *J. Polym. Sci.*, Part A, 1969, vo, 7, p. 183.
33. Volynskii, A.L. and Bakeev, N.F., *Strukturnaya samoorganizatsiya amorfnykh polimerov* (Structural Self-Assembly of Amorphous Polymers), Moscow: Fizmatlit, 2005.
34. Yarysheva, L.M., Rukhlya, E.G., Yarysheva, A.Yu., Volynskii, A.L., and Bakeev, N.F., *Obzorn. Zh. Khim.*, 2012, vol. 2, p. 3.
35. Bowden, P.B. and Raha, S., *Philos. Mag.*, 1970, vol. 22, p. 463.
36. Kinloch, A.J. and Young, R.J., *Fracture Behaviour of Polymers*, Netherlands: Springer, 2013.
37. Arinstein, A. and Zussman, E., *J. Polym. Sci., Part B: Polym. Phys.*, 2011, vol. 49, p. 691.
38. Mohammadzadehmoghadam, S., Dong, Y., and Jeffery Davies, I., *J. Polym. Sci., Part B: Polym. Phys.*, 2015, vol. 53, p. 1171.
39. Sirc, J., Hobzova, R., Kostina, N., Munzarova, M., Juklickova, M., Lhotka, M., Kubinova, S., Zajicova, A., and Michalek, J., http://dx.doi.org/.10.1155/2012/327369.
40. Gupta, P., Elkins, C., Long, T.E., and Wilkes, G.L., *Polymer*, 2005, vol. 46, p. 4799.
41. Kolbuk, D., Sajkiewicz, P., and Kowalewski, T.A., *Eur. Polym. J.*, 2012, vol. 48, p. 275.
42. Stephens, J.S., Frisk, S., Megelski, S., Rabolt, J.F., and Chase, D.B., *Appl. Spectrosc.*, 2001, vol. 55, p. 1287.
43. Hohman, M.M., Shin, M., Rutledge, G., and Brenner, M.P., *Phys. Fluids*, 2001, vol. 13, p. 2201.
44. Shin, Y.M., Hohman, M.M., Brenner, M.P., and Rutledge, G.C., *Polymer*, 2001, vol. 42, p. 09955.
45. Reneker, D.H., Yarin, A.L., Fong, H., and Koombhongse, S., *J. Appl. Phys.*, 2000, vol. 87, p. 4531.
46. Megelski, S., Stephens, J.S., Chase, D.B., and Rabolt, J.F., *Macromolecules*, 2002, vol. 35, p. 8456.
47. Dayal, P., Liu, J., Kumar, S., and Kyu, T., *Macromolecules*, 2007, vol. 40, no. 21, p. 7689.
48. Koombhongse, S., Liu, W., and Reneker, D.H., *J. Polym. Sci., Part B: Polym. Phys.,* 2001, vol. 39, p. 2598.
49. Casper, C.L., Stephens, J.S., Tassi, N.G., Chase, D.B., and Rabolt, J.F., *Macromolecules*, 2004, vol. 37, p. 573.
50. Reneker, D.H., Yarin, A.L., Zussman, E., and Xu, H., *Adv. Appl. Mech.* 2007, vol. 41, p. 43.
51. Thavasi, V., Singh, G., and Ramakrishna, S., *Energy Environ. Sci.*, 2008, vol. 1, p. 205.
52. Wu, H., Zhang, R., Sun, Y., Lin, D., Sun, Z., Pan, W., and Downs, P., *Soft Matter*, 2008, vol. 4, p. 2429.
53. Baker, S.C., Atkin, N., Gunning, P.A., Granville, N., Wilson, K., Wilson, D., and Southgate, J., *Biomaterials*, 2006, vol. 27, p. 3136.
54. Maretschek, S., Greiner, A., and Kissel, T., *J. Control. Release*, 2008, vol. 127, p. 180.
55. Ra, E.J., An, K.H., Kim, K.K., Jeong, S.Y., and Lee, Y.H., *Chem. Phys. Lett.*, 2005, vol. 413, p. 188.

56. Greiner, A. and Wendorff, J.H., *Angew. Chem., Int. Ed. Engl.*, 2007, vol. 46, p. 5670.
57. Chang, C.-C., Huang, C.-M., Chang, Y.-H., and Kuo, C., *Opt. Express*, 2010, vol. 18, no. S2, p. A174.
58. Cuenot, S., Demoustier-Champagne, S., and Nysten, B., *Phys. Rev. Lett.,* 2000, vol. 85, p. 1690.
59. Tan, E.P.S., Goh, C.N., Sow, C.H., and Lim, C.T., *Appl. Phys. Lett.*, 2005, vol. 86, p. 073115.
60. Burman, M., Arinstein, A., and Zussman, E., Appl. *Phys. Lett.*, 2008, vol. 93, p. 193118.
61. Yuya, P.A., Wen, Y., Turner, J.A., Dzenis, Y.A., and Li, Z., *Appl. Phys. Lett.*, 2007, p. 111909.
62. Shin, M.K., Kim, S.I., Kim, S.J., Kim, S.-K., Lee, H., and Spinks, G.M., *Appl. Phys. Lett.*, 2006, vol. 89, p. 231929.
63. Arinstein, A., Burman, M., Gendelman, O., and Zussman, E., *Nat. Nano*, 2007, vol. 2, p. 59.
64. Liu, Y., Li, C., Chen, S., Wachtel, E., Koga, T., Sokolov, J.C., and Rafailovich, M.H., *J. Polym. Sci., Part B: Polym. Phys.*, 2009, vol. 47, p. 2501.
65. Wei, W. and Asa, H.B., *Nanotechnology*, 2010, vol. 21, p. 225701.
66. Hwang, K.Y., Kim, S.-D., Kim, Y.-W., and Yu, W.-R., *Polym. Test.*, 2010, vol. 29, p. 375.
67. Ji, Y., Li, B., Ge, S., Sokolov, J.C., and Rafailovich, M.H., *Langmuir*, 2006, vol. 22, p. 1321.
68. Treloar, L.R.G., *The Physics of Rubber Elasticity*, New York: Clarendon, 2005.
69. Volynskii, A.L. and Bakeev, N.F., *Surface Phenomena in the Structural and Mechanical Behaviour of Solid Polymers*, New York: Taylor & Francis, 2016.
70. Volynskii, A.L. and Bakeev, N.F., *Polym. Sci., Ser. A*, 2009, vol. 51, p. 1096.
71. Volynskii, A.L., Yarysheva, L.M., and Bakeev, N.F., *Polym. Sci., Ser. A*, 2011, vol. 53, p. 871.
72. Glasstone, S., Laidler, K.J., and Eyring, H., *The Theory of Rate Processes*, New York: McGraw-Hill, 1941.
73. Lazurkin, Yu.S. and Fogel'son, R.L., *Zh. Tekh. Fiz.*, 1951, vol. 21, p. 267.
74. Yarysheva, L.M., Pazukhina, L.Yu., Kabanov, N.M., Lukovkin, G.M., Volynskii, A.L., Bakeev, N.F., and Kozlov, P.V., *Vysokomol. Soedin., Ser. A*, 1984, vol. 26, p. 388.
75. Lazurkin, Yu.S., *Doctoral (Phys.-Math.) Dissertation*, Moscow: Inst. of Physical Problems, USSR Acad. Sci., 1954.
76. Bakeev, N.P., Lukovkin, G.M., Marcus, I., Mikouchev, A.E., Shitov, A.N., Vanissum, E.B., and Volynskii, A.L., US Patent 5516473, 1996.
77. Kolluru, P.V. and Chasiotis, I., *Polymer*, 2015, vol. 56, p. 507.
78. Volynskii, A.L., Yarysheva, L.M., and Bakeev, N.F., *Polym. Sci., Ser. A*, 2011, vol. 53, p. 871.

Translated by A. Kirilin